Draft version April 26, 2013
Preprint typeset using LaTeX style emulateapj v. 5/2/11

arXiv:1304.6741v1 [nucl-th] 24 Apr 2013

TABULATED EQUATION OF STATE FOR SUPERNOVA MATTER INCLUDING FULL NUCLEAR ENSEMBLE

N. Buyukcizmeci[1,2], A.S. Botvina[1,3,4], I.N. Mishustin[1,5]
[1]Frankfurt Institute for Advanced Studies, J.W. Goethe University, D-60438 Frankfurt am Main, Germany
[2]Department of Physics, Selcuk University, 42079 Kampus, Konya, Turkey
[3]Institute for Nuclear Research, Russian Academy of Sciences, 117312 Moscow, Russia
[4]Institut für Kernphysik, J. Gutenberg Universität, 55099 Mainz, Germany
[5]Kurchatov Institute, Russian Research Center, 123182 Moscow, Russia.

Draft version April 26, 2013

ABSTRACT

This is an introduction to the equation of state (EOS) for stellar matter at subnuclear densities calculated with the Statistical Model for Supernova Matter (SMSM). Tables for EOS of the supernova matter are constructed for a wide range of the densities $\rho = (10^{-8} - 0.32)\rho_0$, and of the temperatures $T = 0.2 - 25$ MeV for different electron fractions $Y_e = 0.02 - 0.56$. The cases of β-equilibrium are also considered. In this paper we explain the data structure and content of the SMSM EOS tables.

Subject headings: equation of state – nuclear astrophysics, abundances – stars: neutron – supernovae

1. INTRODUCTION

As established in intensive experimental studies of last 20 years, many nuclear reactions lead to the formation of thermalized nuclear systems characterized by subnuclear densities and temperatures of 3-8 MeV. De-excitation of such systems goes through nuclear multifragmentation, i.e. break-up into many excited fragments and nucleons. As it is generally accepted, thermal and chemical equilibrium can be established in many multifragmentation reactions. Transport theoretical calculations of both central heavy-ion collisions around the Fermi-energy and peripheral heavy-ion collisions predicts momentum distributions of nucleons which are similar to equilibrium ones after first ≈ 100 fm/c (see references in the topical issue of Eur. Phys. J. A, 30 (2006)). The final proof of equilibration was provided by numerous comparisons of statistical models with experimental data: These models perfectly describe many characteristics of nuclear fragments observed in multifragmentation experiments: multiplicities of intermediate-mass fragments, charge and isotope distributions, event by event correlations of fragments (including fragments of different sizes), their angular and velocity correlations, and other observables (Gross (1990); Bondorf et al. (1995); Souliotis et al. (2007); Ogul et al. (2011); Botvina, Iljinov, & Mishustin (1990); Botvina et al. (1995); Scharenberg et al. (2001); D'Agostino et al. (1996, 1999); Bellaize et al. (2002); Avdeyev et al. (2002); Hauger et al. (2000); Iglio et al. (2006); Hudan et al. (2009); Wang et al. (1999); Viola et al. (2001); Rodionov et al. (2002); Pienkowski et al. (2002)). The parameters of nuclear matter at the moment of formation of hot fragments, such as temperature and density, can also be established reliably in experiment by using observed relative velocities of fragments, and relative isotope yields.

A nuclear matter at similar conditions is expected in many astrophysical situations, in particular, in supernovae. In order to clarify the thermodynamical conditions obtained in nuclear reactions, we show the phase diagram for symmetric and asymmetric nuclear matter in Fig. 1 (Buyukcizmeci et al. (2013)), for a range of densities and temperatures appropriate for core-collapse supernova explosions. Typical conditions associated with multifragmentation reactions are indicated by the shaded area in Fig. 1. These reactions give us a chance to access hot nuclei in the environment of other nuclear species in thermodynamical equilibrium as we expect in supernova matter. The properties of these nuclei can be directly extracted from experimental data and then this information can be used for more realistic calculations of nuclear composition in stellar matter. This is a new possibility to study this matter besides theoretical approaches which use nuclear forces extracted from experimental study of nuclear structure. As one can estimate from Fig. 1, in the course of massive star collapse the stellar nuclear matter passes exactly through the multifragmentation region with typical entropy per baryon $S/B = 1 - 4$. The electron fraction Y_e, which is equal to the total proton fraction, in the supernova core varies from 0.1 to 0.5. In the two-phase coexistence region (below the solid and dot-dashed lines) at densities $\rho \approx 0.3 - 0.8\rho_0$ the matter should be in a mixed phase, which is strongly inhomogeneous with intermittent dense and dilute regions. In the coexistence region at lower densities, $\rho < 0.3\rho_0$ the nuclear matter breaks up into compact nuclear droplets surrounded by nucleons. These relatively low densities dominate during the main stages of stellar collapse and explosion. Under such conditions one can expect a mixture of nucleons and light and heavy nuclei. In Fig. 1 we demonstrate also isentropic trajectories in nuclear matter (dashed curves) and the trajectories of density and temperature inside the supernova core, which are taken from the supernova simulation of the star with 15 solar masses (Sumiyoshi et al. (2005)) (red dotted curves). The snapshots in the supernova dynamics are selected for three stages before, at, and after the core bounce. In the gravitational collapse from the iron core of the star (BB: just before bounce), the density and temperature roughly follows the isentropic curves S/B=1–2. At the core bounce, when the central density increases just above the nuclear matter density ρ_0, the temperature of

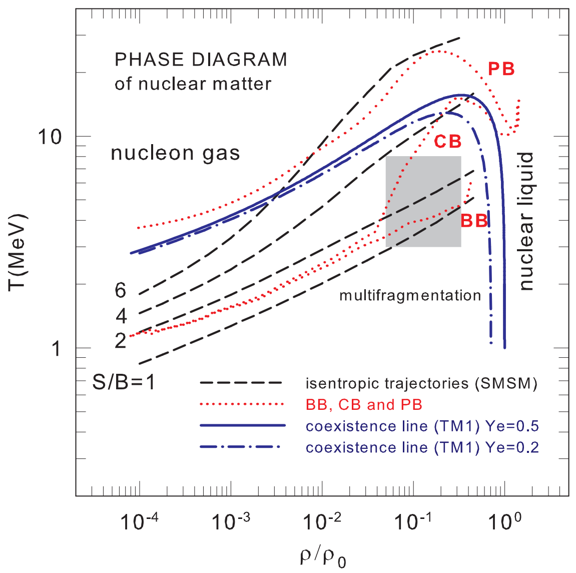

Fig. 1.— Nuclear phase diagram in the 'temperature – baryon density' plane. Solid black and dashed-dotted purple lines indicate boundaries of the liquid-gas coexistence region for symmetric (Lamb et al. (1978)) and asymmetric matter ($Y_e = 0.2$) calculated with TM1 interactions (Sugahara & Toki (1994)). The shaded area corresponds to typical conditions for nuclear multifragmentation reactions. The dashed black lines are isentropic trajectories characterized by constant entropy per baryon, S/B =1, 2, 4 and 6 calculated with SMSM (Botvina & Mishustin (2010)). The dotted red lines show model results of Sumiyoshi et al. (2005) for BB (just before the bounce), CB (at the core bounce) and PB (the post bounce) in a core-collapse supernova. This figure is taken from Buyukcizmeci et al. (2013)(Color version online.).

the inner core becomes higher than 10 MeV due to the passage of the shock wave (CB: core bounce). The temperature of the whole supernova core is still high at 150 ms after the core bounce (PB: post bounce). The shock wave is stalled around 130 km in this 1D calculation, which does not lead to an explosion.

These conditions inside the supernova core pass through interesting regions of the phase diagram. The BB and CB trajectories go through the multifragmentation region, which motivates us to assess the supernova conditions by the multifragmentation reactions taking place in heavy-ion collisions of intermediate energy. The trajectories after the bounce (CB and PB) traverse the phase boundary between the mixture of nuclei and the nucleon gas. This region is dominated by light nuclei (^{4}He and lighter ones) (Botvina & Mishustin (2004); Hempel & Schaffner-Bielich (2010); Hempel et al. (2012); Typel et al. (2010); Hempel et al. (2011); Sumiyoshi & Röpke (2008); Arcones et al. (2008)). Since the dynamics of the shock wave is affected by the interaction of neutrinos with nucleons and nuclei, it is important to determine the composition of hot dense matter in this region by involving into consideration the full ensemble of nuclear species (Botvina & Mishustin (2004)). In fact, the heating through neutrino absorption contributes to the revival of shock wave together with the hydro-dynamical instabilities in 2D and 3D supernova simulations.

2. STATISTITAL MODEL FOR SUPERNOVA MATTER (SMSM)

The Statistical Model for Supernova Matter (SMSM) was first introduced in Ref. (Botvina & Mishustin (2004, 2010)) as generalization of the Statistical Multifragmentation Model (Bondorf et al. (1995)) which was successfully used for description of nuclear multifragmentation reactions (Ogul et al. (2011); Botvina et al. (1995); Scharenberg et al. (2001); D'Agostino et al. (1996, 1999); Bellaize et al. (2002); Avdeyev et al. (2002); Hauger et al. (2000); Iglio et al. (2006); Hudan et al. (2009); Wang et al. (1999); Viola et al. (2001)). This gives us a confidence that this model can realize the approach to diluted stellar matter described in Introduction. We describe supernova matter as a mixture of nuclear species, electrons, photons, and perhaps neutrinos in thermal equilibrium. Below we give the description of model with latest modifications.

2.1. *Equilibrium conditions*

We assume that each particle i with baryon number B_i, charge Q_i and lepton number L_i is characterized by a chemical potential μ_i, which is represented as

$$\mu_i = B_i\mu_B + Q_i\mu_Q + L_i\mu_L. \tag{1}$$

Here μ_B, μ_Q and μ_L are three independent chemical potentials which are determined from the conservation of total baryon number $B = \sum_i B_i$ electric charge $Q = \sum_i Q_i$ and lepton number $L = \sum_i L_i$ of the system. The chemical potentials for nuclear species (A, Z), electrons (e^-, e^+), and neutrinos $(\nu, \tilde{\nu})$ are expressed as

$$\begin{aligned} &\mu_{AZ} = A\mu_B + Z\mu_Q \ , \\ &\mu_{e^-} = -\mu_{e^+} = -\mu_Q + \mu_L \ , \\ &\mu_\nu = -\mu_{\tilde{\nu}} = \mu_L \ . \end{aligned} \tag{2}$$

These relations are valid also for nucleons, $\mu_n = \mu_B$ and $\mu_p = \mu_B + \mu_Q$. The corresponding conservation laws can be written as

$$\begin{gathered} \rho = \frac{B}{V} = \sum_{AZ} A\rho_{AZ} \ , \\ \rho_Q = \frac{Q}{V} = \sum_{AZ} Z\rho_{AZ} - \rho_e = 0 \ , \\ \rho_L = \rho_e + \rho_\nu - \rho_{\tilde{\nu}} = Y_L\rho \ . \end{gathered} \tag{3}$$

Here $\rho_e = \rho_{e^-} - \rho_{e^+}$ is the net electron density, Y_L is the lepton fraction, and V is the normalization volume. The second equation requires that any macroscopic volume of the star (V) is electrically neutral.

The lepton number conservation is a valid concept only if ν and $\tilde{\nu}$ are trapped in the system within the neutrino sphere (Prakash et al. (1997)). If they escape freely from the star, the lepton number conservation is irrelevant and $\mu_L = 0$. In this case two remaining chemical potentials are determined from the conditions of baryon number conservation and electro-neutrality. Since the β-equilibrium may not be achieved in a fast explosive process, we also often fix the electron fraction Y_e in the calculations.

2.2. *Ensemble of nuclear species*

The Grand Canonical version of the SMM (Botvina, Iljinov, & Mishustin (1985)) is used for describing an ensemble of nuclear species under supernova conditions. After integrating out translational degrees of freedom one can write the pressure of nuclear species as

$$P_{\rm nuc} = T \sum_{AZ} \rho_{AZ} \equiv \qquad (4)$$

$$T \sum_{AZ} g_{AZ} \frac{V_f}{V} \frac{A^{3/2}}{\lambda_T^3} \exp\left[-\frac{1}{T} \left(F_{AZ} - \mu_{AZ} \right) \right] ,$$

where ρ_{AZ} is the density of nuclear species with mass A and charge Z. Here g_{AZ} is the ground-state degeneracy factor of species (A,Z), $\lambda_T = \left(2\pi\hbar^2/m_N T\right)^{1/2}$ is the nucleon thermal wavelength, $m_N \approx 939$ MeV is the average nucleon mass. V is the actual volume of the system, and V_f is so called free volume, which accounts for the finite size of nuclear species. We assume that all nuclei have normal nuclear density ρ_0, so that the proper volume of a nucleus with mass A is A/ρ_0. At low densities the finite-size corrections can be included via the excluded volume approximation, $V_f/V \approx (1-\rho/\rho_0)$. This approximation is commonly accepted in statistical models, and it is considered as a reasonable one at the densities $\rho < 0.1\rho_0$. Some information about the free volume at higher densities can be extracted from analysis of experimental data obtained in multifragmentation reactions (Scharenberg et al. (2001)).

The internal excitations of nuclei play an important role in regulating their abundance, since they increase significantly their entropy. Some authors (see, e.g., Ref. (Ishizuka, Ohnishi, & Sumiyoshi (2003))) limit the excitation spectrum by particle-stable levels known for low excited nuclei. Within the SMM we follow quite different philosophy motivated by intensive investigation of disintegration of nuclei at temperatures more than 1 MeV. Namely, we calculate internal excitation of nuclei by assuming that they have the same internal temperature as the surrounding medium. In this case not only particle-stable states but also particle-unstable states will contribute to the excitation energy and entropy. This assumption can be justified by the dynamical equilibrium of nuclei in the hot environment, and is supported by numerous comparisons with experiment (see section **1**). Moreover, in the supernova environment both the excited states and the binding energies of nuclei will be strongly affected by the surrounding matter. By this reason, we find it more appropriate to use an approach which can easily be generalized to include in-medium modifications.The internal free energy of species (A,Z) with $A > 4$ is parameterized in the spirit of the liquid drop model, which has been proved to be very successful in nuclear physics (Bohr (1936); Bondorf et al. (1995)):

$$F_{AZ}(T,\rho) = F_{AZ}^B + F_{AZ}^S + F_{AZ}^{\rm sym} + F_{AZ}^C \quad . \qquad (5)$$

Here the right hand side contains, respectively, the bulk, the surface, the symmetry and the Coulomb terms. The first three terms are taken in the standard form (Bondorf et al. (1995)),

$$F_{AZ}^B(T) = \left(-w_0 - \frac{T^2}{\varepsilon_0} \right) A \quad , \qquad (6)$$

$$F_{AZ}^S(T) = \beta_0 \left(\frac{T_c^2 - T^2}{T_c^2 + T^2} \right)^{5/4} A^{2/3} \quad , \qquad (7)$$

$$F_{AZ}^{\rm sym} = \gamma \frac{(A-2Z)^2}{A} \quad , \qquad (8)$$

where $w_0 = 16$ MeV, $\varepsilon_0 = 16$ MeV, $\beta_0 = 18$ MeV, $T_c = 18$ MeV and $\gamma = 25$ MeV are the model parameters which are extracted from nuclear phenomenology and provide a good description of multifragmentation data (Bondorf et al. (1995); Botvina et al. (1995); Scharenberg et al. (2001); D'Agostino et al. (1996); Bellaize et al. (2002); Avdeyev et al. (2002); D'Agostino et al. (1999)). However, these parameters, especially the symmetry coefficient γ, can be different in hot nuclei at multifragmentation conditions, and they should be determined from corresponding experimental data (see discussion in Refs. (Botvina et al. (2006); Buyukcizmeci et al. (2008); Botvina, Lozhkin, & Trautmann (2002))).

In the electrically-neutral environment the nuclear Coulomb term should be modified to include the screening effect of electrons. This can be done, e.g., within the Wigner-Seitz approximation as was discussed in Ref. (Lamb, Lattimer, & Pethick (1981); Lattimer et al. (1985)). We divide the whole system into spherical cells each containing one nucleus. The radius of the cell is determined by the condition that it contains the same number of electrons as the number of protons in the nucleus. Then assuming a constant electron density we obtain

$$F_{AZ}^C(\rho) = \frac{3}{5} c(\rho) \frac{(eZ)^2}{r_0 A^{1/3}} \quad , \qquad (9)$$

$$c(\rho) = \left[1 - \frac{3}{2} \left(\frac{\rho_e}{\rho_{0p}} \right)^{1/3} + \frac{1}{2} \left(\frac{\rho_e}{\rho_{0p}} \right) \right] ,$$

where $r_0 = 1.17$ fm and $\rho_{0p} = (Z/A)\rho_0$ is the proton density inside the nuclei. The screening function $c(\rho)$ is 1 at $\rho_e = 0$ and 0 at $\rho_e = \rho_{0p}$. To simplify calculations we often use an approximation $\rho_e/\rho_{0p} = \rho/\rho_0$, as in Ref. (Lamb, Lattimer, & Pethick (1981); Lattimer et al. (1985)), which works well when neutrons mostly bound in nuclei, and leads to very similar results in many cases. We want to stress that the reduction of the Coulomb energy due to the electron screening favors the formation of heavy nuclei. Nucleons and light nuclei ($A \leq 4$) are considered as structure-less particles characterized only by exact masses and proper volumes (Bondorf et al. (1995)). Their Coulomb interaction is taken into account within the same Wigner-Seitz approximation.

In Fig. 2, we present the pure nuclear pressure P_{nuc} (Eq. (4)) caused by single nucleons and nuclei produced after clusterization of nucleons. In addition, in the supernova environment free electrons existing together with nuclear clusters modify the Coulomb energy and lead to a negative contribution to pressure (Baym, Pethick, & Sutherland (1971)). The physical

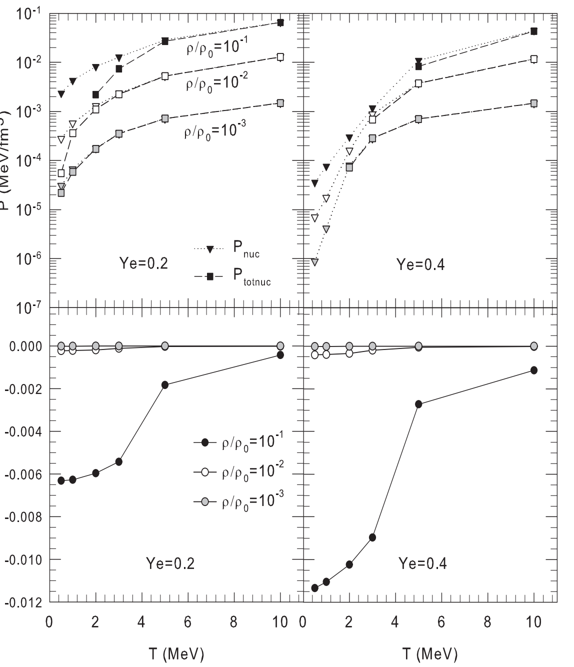

FIG. 2.— Comparison of results for the Coulomb contribution P_C(bottom panels), pure P_{nuc} and total nuclear pressure P_{totnuc} (top panels) as a function of temperature for $Y_e = 0.2$, 0.4 and $\rho/\rho_0 = 10^{-1} - 10^{-3}$.

reason is that electrons compensate the positive charge of nuclei, and the Coulomb energy of Wigner-Seitz cells decrease when the density increases. This Coulomb contribution can be calculated as:

$$P_C = \rho \sum_{AZ} \rho_{AZ} \frac{\partial F^C_{AZ}}{\partial \rho}, \qquad (10)$$

where the expression (9) for F^C_{AZ} is used. The total nuclear pressure P_{totnuc} , which is the sum of the pure nuclear pressure P_{nuc} and P_C, is demonstrated in Fig. 2 as a function of temperature. It is important that at $T \geqslant 5$ MeV, when matter nearly completely dissociates into nucleons and lightest clusters, P_C is close to zero. In this region the total nuclear pressure coincides with the pure nuclear pressure. The Coulomb pressure becomes very important when heavy clusters dominate in the system. One can see in Fig. 2 that at low temperatures and high density the total nuclear pressure may be negative. In this case the nuclear clusterization is favorable for the collapse. However, the positive pressure of the relativistic degenerate electron Fermi-gas is considerably (more than an order of magnitude) larger. Therefore the total pressure $P_{\rm tot}$ given by the sum of the total nuclear, electron and photon pressures in such environment will always be positive and the condition of thermodynamical stability ($\partial P^{\rm tot}/\partial\rho \geq 0$) will be fulfilled.

As follows from Eq. (4), the fate of heavy nuclei depends strongly on the relationship between F_{AZ} and μ_{AZ}. In order to avoid an exponentially divergent contribution to the baryon density, at least in the thermodynamic limit ($A \to \infty$), inequality $F_{AZ} \geqslant \mu_{AZ}$ must hold. The equality sign here corresponds to the situation when a big (infinite) nuclear fragment coexists with the gas of smaller clusters (Bugaev, Gorenstein, & Mishustin (2001)). When $F_{AZ} > \mu_{AZ}$, only small clusters with nearly exponential mass spectrum are present. However, there exists a region of thermodynamic quantities corresponding to $F_{AZ} \approx \mu_{AZ}$ when the mass distribution of nuclear species is close to a power-law $A^{-\tau}$ with $\tau \approx 2$. This is a characteristic feature of the liquid-gas phase transition. The advantage of our approach is that we consider all the fragments present in this transition region, and, therefore, can study this phase transition in all details.

2.3. *Leptons and photons*

Besides nuclear species the supernova matter contains leptons (e^-, e^+, ν_e, $\tilde{\nu_e}$, ...) and photons. At $T, \mu > m_e$ the pressure of the relativistic electron-positron gas can be written as

$$P_e = \frac{g_e \mu_e^4}{24\pi^2} \cdot \qquad (11)$$
$$\left[1 + 2\left(\frac{\pi T}{\mu_e}\right)^2 + \frac{7}{15}\left(\frac{\pi T}{\mu_e}\right)^4 - \frac{m_e^2}{\mu_e^2}\left(3 + \left(\frac{\pi T}{\mu_e}\right)^2\right)\right],$$

where first-order correction ($\sim m_e^2$) due to the finite electron mass is included, g_e=2 is the spin degeneracy factor for electrons. The net number density ρ_e and entropy density s_e can be obtained from standard thermodynamic relations, $\rho_e = \partial P_e/\partial\mu_e$, and $s_e = \partial P_e/\partial T$, which give

$$\rho_e = \frac{g_e}{6\pi^2}\left[\mu_e^3 + \mu_e\left(\pi^2 T^2 - \frac{3}{2}m_e^2\right)\right] \ , \qquad (12)$$

$$s_e = \frac{g_e T \mu_e^2}{6}\left[1 + \frac{7}{15}\left(\frac{\pi T}{\mu_e}\right)^2 - \frac{m_e^2}{2\mu_e^2}\right] \ . \qquad (13)$$

Electron neutrinos and anti-neutrinos are taken into account in the same way, but as massless fermions, with the degeneracy factor twice smaller than for the electrons, i.e., g_ν=1. The photons are always close to the thermal equilibrium, and they are treated as massless Bose gas with zero chemical potential. The corresponding density ρ_γ, energy density e_γ, pressure P_γ, and entropy density s_γ of photons are given by standard formulae:

$$\rho_\gamma = \frac{g_\gamma \xi(3) T^3}{\pi^2 \hbar^3 c^3} \ , \ e_\gamma = \frac{g_\gamma \pi^2 T^4}{30\hbar^3 c^3} \ , \ P_\gamma = \frac{e_\gamma}{3} \ , \ s_\gamma = \frac{4 e_\gamma}{3T}, \qquad (14)$$

where g_γ=2.

3. THE SMSM EOS TABLES

We have constructed the SMSM EOS tables which are available on the Web at *http://fias.uni-frankfurt.de/physics/mishus/research/smsm/*. Below we will give the detailed information about mess of tables, entries and application of EOS tables.

3.1. *Mesh of the SMSM EOS Tables*

The SMSM EOS tables cover the following range:

- **Temperature:** $T = 0.2 - 25$ MeV; for 35 T values.
- **Electron fraction Y_e:** $0.02 - 0.56$; linear mesh of $Y_e = 0.02$, giving 28 Y_e values. It is equal to the total proton fraction X_p, due to charge neutrality.

TABLE 1
Temperature, electron fraction and density fraction values of SMSM EOS tables.

			T(MeV)			
0.20	0.40	0.60	0.80	1.00	1.25	1.50
1.75	2.00	2.25	2.50	2.75	3.00	3.25
3.50	3.75	4.00	4.25	4.50	4.75	5.00
5.25	5.50	5.75	6.00	6.50	7.00	7.50
8.00	9.00	10.00	12.00	15.00	20.00	25.00
			Y_e			
0.02	0.04	0.06	0.08	0.10	0.12	0.14
0.16	0.18	0.20	0.22	0.24	0.26	0.28
0.30	0.32	0.34	0.36	0.38	0.40	0.42
0.44	0.46	0.48	0.50	0.52	0.54	0.56
			ρ/ρ_0			
1E-8	1.78E-8	3.16E-8	5.62E-8	1E-7	1.78E-7	3.16E-7
5.62E-7	1E-6	1.78E-6	3.16E-6	5.62E-6	1E-5	1.78E-5
3.16E-5	5.62E-5	1E-4	1.78E-4	3.16E-4	5.62E-4	1E-3
1.78E-3	3.16E-3	5.62E-3	1E-2	1.78E-2	3.16E-2	5.62E-2
		1E-1	1.78E-1	3.16E-1		

TABLE 2
SMSM EOS Tables are available in a machine-readable form in the online journal.

Column1 Y_e	Column2 ρ/ρ_0	Column3 X_n	Column4 X_p	Column5 X_d
0.02	0.100E-07	0.9447	0.3514E-38	0.1248E-35
0.02	0.178E-07	0.9445	0.7178E-39	0.4502E-36
0.02	0.316E-07	0.9442	0.1388E-39	0.1609E-36
Column6 X_t	Column7 $X_{3_{He}}$	Column8 X_{alpha}	Column9 X_{heavy}	Column10 $< A >$
0.2067E-26	0	0.2873E-24	0.05529	89.66
0.1327E-26	0	0.6668E-25	0.05553	90.70
0.8426E-27	0	0.1519E-25	0.05582	91.76
Column11 E_{tot} (MeV)	Column12 E_{nuc} (MeV)	Column13 S_{tot} (k_B)	Column14 S_{nuc} (k_B)	Column15 P_{tot} (MeVfm^{-3})
0.08460	-0.1660	13.81	12.12	0.4077E-09
-0.02699	-0.1666	12.53	11.58	0.6277E-09
-0.09008	-0.1674	11.57	11.03	0.1019E-08
Column16 P_{totnuc} (MeVfm^{-3})	Column17 μ_e (MeV)	Column18 μ_B (MeV)	Column19 μ_Q (MeV)	
0.2816E-09	0.01716	-2.063	-16.96	
0.5011E-09	0.03048	-1.948	-17.28	
0.8906E-09	0.05394	-1.833	-17.60	

- **Baryon number density fraction** $\rho/\rho_0 = (10^{-8} - 0.32)$, giving 31 ρ/ρ_0 values.

The different T (35 points) , ρ/ρ_0 (31 points) and Y_e (28 points) values sum up to 30380 EOS grid points are presented in the Table 1. We believe that the physics of SMSM EOS is sufficiently well presented with our grid points. Running time for calculations was approximately 7.8 days (Work station:4xDual core AMD 2.2 GHz processor). We have obtained *SMSM-Tables.txt*, the size of this file 6.3 MB, it contains 31493 lines.

3.2. *Description of the SMSM EOS Tables*

The information is stored in a format which is very similar to the tables of Shen et al. (1998) or Hempel & Schaffner-Bielich (2010) or Furusawa et al. (2011) so that it can easily be implemented in running codes. The SMSM EOS tables file under the name *"SMSM-Tables.txt"* is the main file which is available in the online journal.

In the beginning of file we write the general parameters of liquid-drop description: $W_0 = 16$ MeV, $B_0 = 18$ MeV, $T_c = 18$ MeV, $\gamma = 25$ MeV, $\varepsilon_0 = 16$ MeV, $r_0 = 1.17$ fm. The tables are written in the order of increasing T. In the tables, the values of T (MeV) are given at the beginning of each block, and the blocks with different T are divided by the string of characters *cccccc*. For each T, we present the results in the order of increasing Y_e and ρ/ρ_0 (see Table 1). We put also space lines between Y_e blocks. A portion of the quantities in one line of SMSM EOS Tables are shown in Table 2 for guidance regarding its form and content. The quantities in one line of table for each density grid point the 19 different thermodynamic quantities are listed and defined as follows:

1. Y_e, electron fraction: $Y_e = \rho_e/\rho$,
2. ρ/ρ_0, density fraction ,
3. X_n, neutron fraction: $X_n = \rho_n/\rho$,
4. X_p, proton fraction: $X_p = \rho_p/\rho$,
5. X_d, doterium fraction: $X_d = \rho_d/\rho$,
6. X_t, tritium fraction: $X_t = \rho_t/\rho$,
7. $X_{^3He}$, ^{3}He fraction: $X_{^3He} = \rho_{^3He}/\rho$,
8. X_{alpha}, alpha fraction $X_{alpha} = \rho_{alpha}/\rho$,
9. X_{heavy}, heavy fragments ($A > 4$) fraction, $X_{heavy} = \rho_{heavy}/\rho$,
10. $< A >$, average mass number of heaviest fragment ,
11. E_{tot}, total energy is the sum of nuclear E_{nuc}, electron E_e and photon E_{photon} entropy contributions. $E_{tot} = E_{nuc} + E_e + E_n + E_{photon}$, (MeV/n) ,
12. E_{nuc}, nuclear energy, (MeV/n) ,
13. S_{tot}, total entropy is the sum of nuclear S_{nuc}, electron S_e and photon S_{photon} entropy contributions. $S_{tot} = S_{nuc} + S_e + S_n + S_{photon}$, ($k_B$) ,
14. S_{nuc}, nuclear entropy, (k_B) ,
15. P_{tot}, total pressure is the sum of the pressure of nuclear species $P_{\rm totnuc}$, electrons $P_{\rm e}$, neutrons $P_{\rm n}$ and photons $P_{\rm photon}$, (MeVfm^{-3}) ,
$$P_{\rm tot} = P_{\rm totnuc} + P_{\rm e} + P_{\rm n} + P_{\rm photon} \ ,$$
16. $P_{\rm totnuc}$, total nuclear pressure, (MeVfm^{-3}) ,
$$P_{\rm totnuc} = P_{\rm nuc} + P_{\rm C} \ ,$$
17. μ_e, chemical potential of electrons, (MeV) ,
18. μ_B, chemical potential of mass number, (MeV) ,
19. μ_Q, chemical potential of charge, (MeV) .

3.3. *Application of the EOS tables and illustrative results*

In addition to standard output (the 19 different thermodynamic quantities), like the pressure, entropy energy, fractions of few light particles and heavy nuclei (actually in Shen et al. (1998) case a single heavy nucleus), we provide a possibility to extract the ensemble of all heavy nuclei. We are doing it by providing the chemical potentials and the formula

$$< \rho_{AZ} >= g^0_{AZ}(1-\frac{\rho}{\rho_0})\frac{A^{3/2}}{\lambda^3_T} \cdot \qquad (15)$$

$$\exp\left[-\frac{1}{T}\left(F_{AZ}-\mu_{AZ}\right)\right] ,$$

which is general for all points, and which can calculate densities of nuclei with all mass numbers and charges. We believe that in simulations it could be quite helpful to have knowledge about all heavy nuclei at each points, since weak reactions (with neutrinos and electrons) can be calculated much more precisely with the ensemble of heavy nuclei. Thus, one can easily calculate the the ensemble of all heavy nuclei of stellar matter using this formula and table parameters.

The mass distributions contain important information about fragmentation of matter in the nuclear liquid-gas phase transition (coexistence region). The concept of statistical equilibrium assumes a continuous interaction between fragments via specific microscopic processes, like absorption and emission of neutrons, which provide equilibration (see, e.g., discussion in Ref. (Botvina & Mishustin (2010))). In this situation the nuclei can remain hot and have modified properties and masses, which are different from the cold isolated nuclei. We should note that it is stored also *"SMSM-Relative-Mass-Yield.dat"* data file for mass distributions of system for each calculations to make quick check one by one for us. This file size is 356 MB, it contains 30380 lines and every line has 1000 column (A=1-1000). Since we have 35 T and 28 Y_e values, (35(T) x 28 (Y_e)=980 values for 31 ρ/ρ_0 values), we grouped 4 density intervals from lower to higher as

- Density-1=$\rho/\rho_0 = 10^{-8} - 5.62.10^{-7}$ (8 values),
- Density-2=$\rho/\rho_0 = 10^{-6} - 5.62.10^{-5}$ (8 values),
- Density-3=$\rho/\rho_0 = 10^{-4} - 5.62.10^{-3}$ (8 values),
- Density-4=$\rho/\rho_0 = 10^{-2} - 3.17.10^{-1}$ (7 values).

Using these interval for data, we have plotted 3920 figures as eps files which contains information about mass distributions of system for each grid point. We have presented example figures for $T = 1$, and 3 MeV, $Y_e = 0.2 - 0.4$ and different densities in Figs. 3, 4, 5 and 6. As seen in these figures, we also put X_n, X_p, X_{alpha}, Y_{heavy}, $< A >$, $\mu_A (= \mu_B)$ and $\mu_Z (= \mu_Q)$ values from tables with the same order of ρ/ρ_0 as the control parameters inside of figures. These figures are presented on the SMSM web page with

- *SMSM-Massdist-Figs-Density-1.zip,*
- *SMSM-Massdist-Figs-Density-2.zip,*
- *SMSM-Massdist-Figs-Density-3.zip,*
- *SMSM-Massdist-Figs-Density-4.zip*

files, each file contains 980 eps figures. For example, inside *SMSM-Massdist-Figs-Density-4.zip* file, one can find mass distribution figure for $T = 1$ MeV, $Y_e = 0.20$ and $\rho/\rho_0 = 10^{-2} - 3.17.10^{-1}$ in *T-1-Ye-020-DENSITY-4.eps* file as shown in Fig. 3.

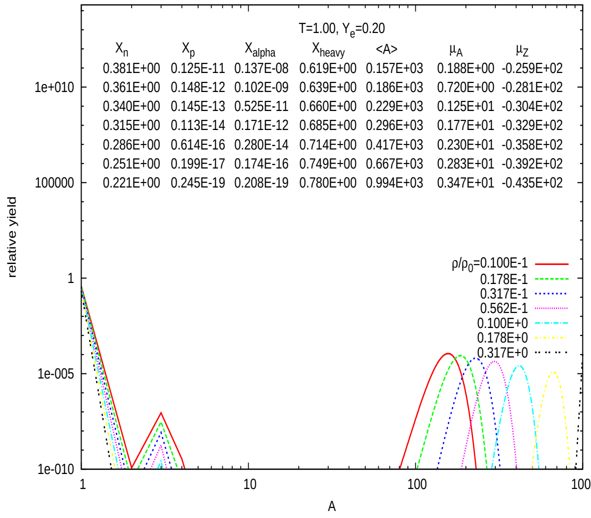

X_n	X_p	X_{alpha}	X_{heavy}	<A>	μ_A	μ_Z
0.381E+00	0.125E-11	0.137E-08	0.619E+00	0.157E+03	0.188E+00	-0.259E+02
0.361E+00	0.148E-12	0.102E-09	0.639E+00	0.186E+03	0.720E+00	-0.281E+02
0.340E+00	0.145E-13	0.525E-11	0.660E+00	0.229E+03	0.125E+01	-0.304E+02
0.315E+00	0.113E-14	0.171E-12	0.685E+00	0.296E+03	0.177E+01	-0.329E+02
0.286E+00	0.614E-16	0.280E-14	0.714E+00	0.417E+03	0.230E+01	-0.358E+02
0.251E+00	0.199E-17	0.174E-16	0.749E+00	0.667E+03	0.283E+01	-0.392E+02
0.221E+00	0.245E-19	0.208E-19	0.780E+00	0.994E+03	0.347E+01	-0.435E+02

FIG. 3.— Mass distributions of fragments produced in matter with temperatures $T = 1$ MeV, electron fractions $Y_e = 0.2$ and densities $\rho/\rho_0 = 10^{-2}-3.17.10^{-1}$. (Color version online.)

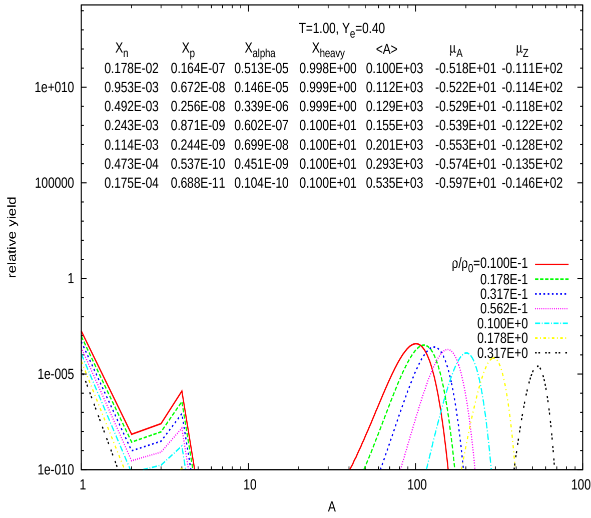

X_n	X_p	X_{alpha}	X_{heavy}	<A>	μ_A	μ_Z
0.178E-02	0.164E-07	0.513E-05	0.998E+00	0.100E+03	-0.518E+01	-0.111E+02
0.953E-03	0.672E-08	0.146E-05	0.999E+00	0.112E+03	-0.522E+01	-0.114E+02
0.492E-03	0.256E-08	0.339E-06	0.999E+00	0.129E+03	-0.529E+01	-0.118E+02
0.243E-03	0.871E-09	0.602E-07	0.100E+01	0.155E+03	-0.539E+01	-0.122E+02
0.114E-03	0.244E-09	0.699E-08	0.100E+01	0.201E+03	-0.553E+01	-0.128E+02
0.473E-04	0.537E-10	0.451E-09	0.100E+01	0.293E+03	-0.574E+01	-0.135E+02
0.175E-04	0.688E-11	0.104E-10	0.100E+01	0.535E+03	-0.597E+01	-0.146E+02

FIG. 4.— The same as Fig. 3 but at $Y_e = 0.4$.

At very low temperatures the SMSM predicts a Gaussian-like distribution for heavy nuclei as seen in Figs. 3 and 4. In this case an approximation of a single heavy nucleus adopted in the Lattimer & Swesty (1991) and Shen et al. (1998) EOSs may work reasonably well for calculations of thermodynamical characteristics of matter. However, already at $T \geq 1$ MeV the gap between the Gaussian peak and light clusters and nucleons is essentially filled by nuclei of intermediate masses leading to characteristic U-shaped distributions. The examples of such distributions are shown in Figs. 5 and 6. They give a typical evolution of mass distributions of nuclei in the coexistence region of the liquid gas phase transition. Previously it was demonstrated for disintegration of finite nuclei (Bondorf et al. (1995)). These distribu-

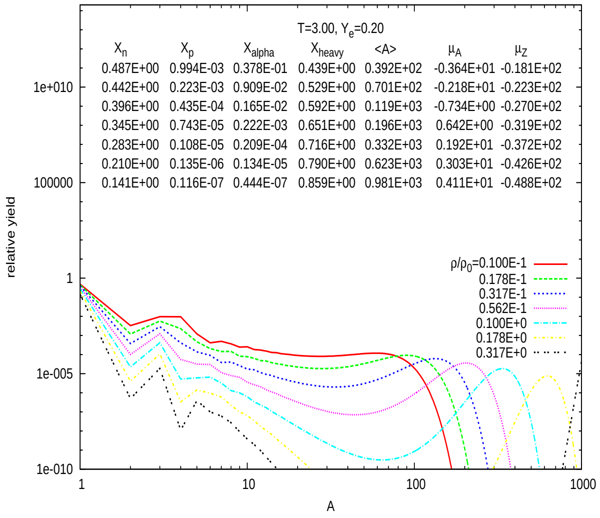
T=3.00, Y_e=0.20

X_n	X_p	X_{alpha}	X_{heavy}	<A>	μ_A	μ_Z
0.487E+00	0.994E-03	0.378E-01	0.439E+00	0.392E+02	-0.364E+01	-0.181E+02
0.442E+00	0.223E-03	0.909E-02	0.529E+00	0.701E+02	-0.218E+01	-0.223E+02
0.396E+00	0.435E-04	0.165E-02	0.592E+00	0.119E+03	-0.734E+00	-0.270E+02
0.345E+00	0.743E-05	0.222E-03	0.651E+00	0.196E+03	0.642E+00	-0.319E+02
0.283E+00	0.108E-05	0.209E-04	0.716E+00	0.332E+03	0.192E+01	-0.372E+02
0.210E+00	0.135E-06	0.134E-05	0.790E+00	0.623E+03	0.303E+01	-0.426E+02
0.141E+00	0.116E-07	0.444E-07	0.859E+00	0.981E+03	0.411E+01	-0.488E+02

FIG. 5.— The same as Fig. 3 but at $T = 3$ MeV.

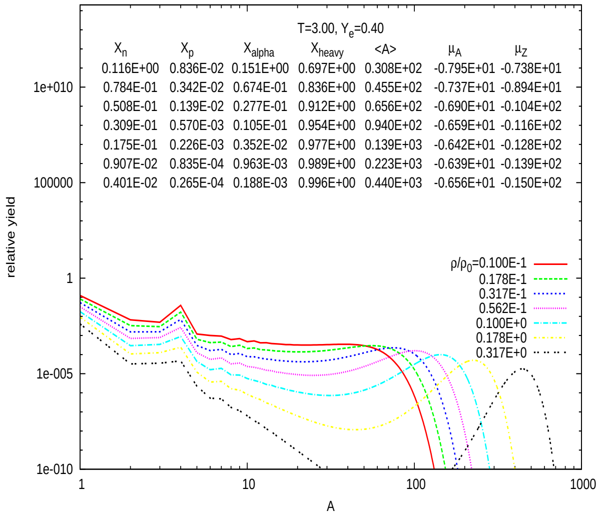
T=3.00, Y_e=0.40

X_n	X_p	X_{alpha}	X_{heavy}	<A>	μ_A	μ_Z
0.116E+00	0.836E-02	0.151E+00	0.697E+00	0.308E+02	-0.795E+01	-0.738E+01
0.784E-01	0.342E-02	0.674E-01	0.836E+00	0.455E+02	-0.737E+01	-0.894E+01
0.508E-01	0.139E-02	0.277E-01	0.912E+00	0.656E+02	-0.690E+01	-0.104E+02
0.309E-01	0.570E-03	0.105E-01	0.954E+00	0.940E+02	-0.659E+01	-0.116E+02
0.175E-01	0.226E-03	0.352E-02	0.977E+00	0.139E+03	-0.642E+01	-0.128E+02
0.907E-02	0.835E-04	0.963E-03	0.989E+00	0.223E+03	-0.639E+01	-0.139E+02
0.401E-02	0.265E-04	0.188E-03	0.996E+00	0.440E+03	-0.656E+01	-0.150E+02

FIG. 6.— The same as Fig. 5 but at $Y_e = 0.4$.

tions continuously transform with decreasing density as well as with increasing temperatures into exponential fall of fragment yields with A.

Information about isotopic yields helps to understand the differences observed for summed quantities like mass yields or mass fractions. It is also possible to obtain isotopic distributions of stellar matter using SMSM EOS tables and Eq. (15). Here, we have shown examples from isotopic distributions of $Z = 8$ and $Z = 26$ in Fig. 7. As seen from these figures, the SMSM gives Gaussian type distributions, which are the consequence of the liquid-drop description of fragments.

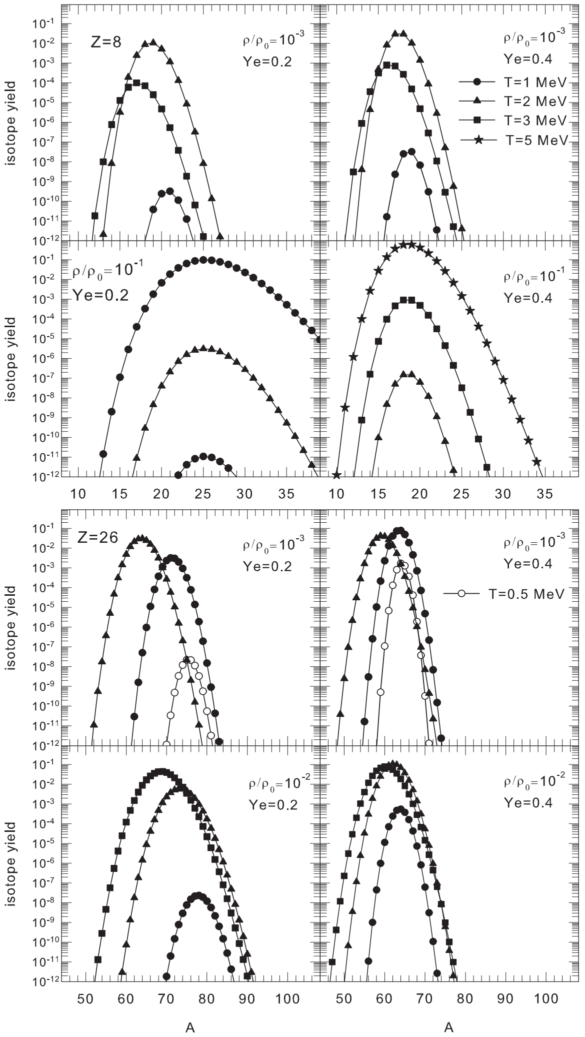

FIG. 7.— Isotopic distributions of $Z = 8$ and $Z = 26$ fragments produced in matter with temperatures $T = 1, 2, 3,$ and 5 MeV, electron fractions $Y_e = 0.2$ and 0.4, densities $\rho/\rho_0 = 10^{-3} - 10^{-1}$.

Recently, we have compared mass and isotope distributions of SMSM (Botvina & Mishustin (2010)), Hempel & Schaffner-Bielich (2010) and Furusawa et al. (2011) EOS models at subnuclear densities, $Y_e = 0.2, 0, 4$, temperatures (0.5-10 MeV) expected to occur during the collapse of massive stars and supernova explosions in Ref. Buyukcizmeci et al. (2013), presently, we have found significant differences between mass distributions of SMSM, HS and FYSS models, which use different assumptions on properties of fragments, especially at low electron fractions, low temperatures and high densities. We note that these differences are also shown in the behaviour of nuclear pressure, see Fig. 22 in Ref. Buyukcizmeci et al. (2013).

3.4. *Nuclear composition under condition of β-equilibrium in stellar matter*

An important case when full β-equilibrium can be reached in matter (see Eq. (2)). One can expect it in some processes like slow collapse of massive stars, in crust of neutron stars, and in some conditions of stellar matter after supernova explosions. On the other hand, the β-equilibrium can be a useful physical limit for theoretical estimate of the nuclear composition without full knowledge of weak reactions. The SMSM allows for this kind of calculations (Botvina & Mishustin (2004, 2010)) and the corresponding Tables, at baryon densi-

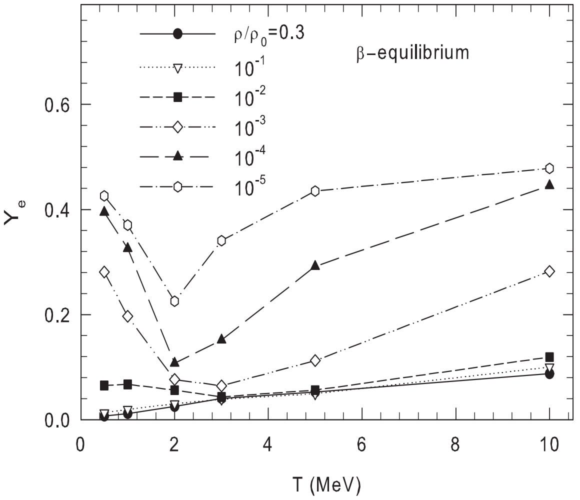

FIG. 8.— Electron fractions in β-equilibrium case versus temperature at densities $\rho/\rho_0 = 0.3 - 10^{-5}$.

ties $\rho = (10^{-8} - 0.32)\rho_0$, and temperatures $T = 0.2 - 25$, are under construction. In this case the corresponding electron fraction Y_e can be systematically found at given ρ and T. In the following this Y_e may be used in standard SMSM tables too. In Fig. 8 we show the calculated electron fraction under β-equilibrium condition for some densities versus temperature. One can see an interesting behavior: There is a trend of increasing Y_e at large temperatures, which has a simple explanation: At high T the constraint imposed on electrons by their large chemical potentials (at high densities) becomes weaker. At the largest density ($\rho = 0.3\rho_0$), when heavy nuclei always present in the ensemble at all temperatures, this trend is permanent. However, at smaller densities ($\rho \leqslant 0.01\rho_0$) the heavy nuclei can exist only at low temperatures since they disintegrate into nucleons and light clusters at high temperatures ($T > 3 - 5$ MeV). These nuclei have big charges and present in a large amount, that requires also a large number of electrons at large temperature. As a result, at such densities there is a temperature at which the electron fraction has a minimum, corresponding to transition from heavy nuclei to free nucleons and light clusters. This is a very instructive effect of coupling of nuclear composition and electron fraction in matter.

4. CONCLUSIONS

We have presented the constructed SMSM EOS tables which give comprehensive information on physical properties of stellar matter at subnuclear densities, temperatures $T < 25$ MeV and electron fractions between 0.02 and 0.56. The SMSM EOS can be used for hydrodynamical simulations of massive stars collapse and supernova explosion processes. We describe the whole ensemble of nuclei, without any artificial limitation of their masses and charges, and general characteristics of matter, like temperature and chemical potentials. The nuclear mass and isotope distributions are needed for realistic calculations of electron capture and neutrino induced reactions. As we have noted the present EOS at large densities as directly related to nuclear multifragmentation reactions, and the properties of nuclei embedded in dense surrounding can be taken by obtained from analysis of these reactions. Our calculations of the thermodynamical parameters and nuclear composition of matter is especially instructive in the case of β-equilibrium. A special case of β-equilibrated nuclear matter is considered too. In particular, we have found non-monotonous behavior of the electron fraction as a function of temperature at $\rho < 0.1\rho_0$. This effect is connected with the rearrangement of the fragment mass distribution from U-shape to exponential fall-off. These results can be used for modeling proto-neutron stars and crusts of neutron stars. We believe that using EOS developed by different groups of authors is crucially important for evaluating real behavior of stellar matter.

5. ACKNOWLEDGEMENT

N.B. and A.S.B. are grateful to Frankfurt Institute for Advanced Studies (FIAS) for support and hospitality. This work is supported by the Helmholtz International Center for FAIR within the LOEWE program. N.B. thanks Selcuk University-Scientific Research Projects (BAP) for partly support. N.B. acknowledges that a part of the numerical calculations were carried out on the computers at Physics Department in Selcuk University. N.B. thanks to R.Ogul for encouragement, A.E.Kavruk and T.Ozturk for the help for the usage of computers in S.U.. A.S.B. acknowledges the support by the Research Infrastructure Integrating Activity 'Study of Strongly Integrating Matter' HadronPhysics3 under the 7th Framework Programme of EU. I.N.M. acknowledges support from the grant NSH-2015.2012.2 (Russia).

REFERENCES

Arcones, A., Martínez-Pinedo, G., O'Connor, E. et al. 2008, *Phys. Rev. C*, 78, 015806
Avdeyev, S. P., Karnaukhov, V. A., Petrov, L. A. et al. 2002, *Nucl. Phys. A*, 709, 392
Baym, G., Pethick, C., & Sutherland, P. 1971, *ApJ*, 170, 299
Bellaize, N., Lopez, O., Wieleczko, J. P. et al. 2002, *Nucl. Phys. A*, 709, 367
Bohr, N. 1936, *Nature*, 137, 344
Bondorf, J. P., Botvina, A. S., Iljinov, A. S., Mishustin, I. N., & Sneppen, K. 1995, *Phys. Rep.*, 257, 133
Botvina, A. S., Iljinov, A. S., & Mishustin, I. N. 1985, *Sov. J. Nucl. Phys.*, 42, 712
Botvina, A. S., Iljinov, A. S., & Mishustin, I. N. 1990, *Nucl. Phys. A*, 507, 649
Botvina, A. S., Mishustin, I. N., Begemann-Blaich, M. et al. 1995, *Nucl. Phys. A*, 584, 737
Botvina, A. S., Lozhkin, O. V., & Trautmann, W. 2002, *Phys. Rev. C*, 65, 044610
Botvina, A. S. & Mishustin, I. N. 2004, *Phys. Lett. B*, 584, 233
Botvina, A. S., Buyukcizmeci, N., Erdogan, M. et al. 2006, *Phys. Rev. C*, 74, 044609
Botvina, A. S. & Mishustin, I. N. 2010, *Nucl. Phys. A*, 843, 98
Bugaev, K. A., Gorenstein, M. I., & Mishustin, I. N. 2001, *Phys. Lett. B*, 498, 144
Buyukcizmeci, N., Botvina A. S., Mishustin I. N., & Ogul, R. 2008, *Phys. Rev. C*, 77, 034608
Buyukcizmeci, N., Botvina, A. S., Mishustin I. N. et al. 2013, *Nucl. Phys. A*, 907, 13
D'Agostino, M., Botvina, A. S., Milazzo, P. M. et al. 1996, *Phys. Lett. B*, 371, 175
D'Agostino, M., Botvina, A. S., Bruno, M. et al. 1999, *Nucl. Phys. A*, 650, 329
Dynamics and Thermodynamics with Nuclear Degrees of Freedom, ed. by Chomaz, Ph., Gulminelli, F., Trautmann, W., & Yennello, S. J. (Springer, Berlin/Heidelberg/New York) 2006, *Eur. Phys. J. A*, 30

Furusawa, S., Yamada, S., Sumiyoshi, K., & Suzuki, H. 2011, *ApJ*, 738, 178

Gross, D. H. E. 1990, *Rep. Prog. Phys.*, 53, 605

Hauger, J. A., Srivastava, B. K., Albergo, S. et al. 2000, *Phys. Rev. C*, 62, 024616

Hempel, M. & Schaffner-Bielich, J. 2010, *Nucl. Phys. A*, 837, 210

Hempel, M., Schaffner-Bielich, J., Typel, S., & Röpke, G. 2011, *Phys. Rev. C*, 84, 055804

Hempel, M., Fisher, T., Schaffner-Bielich, J., & Liebendörfer, M. 2012, *Astrophys. J.*, 70, 748

Hudan, S., McIntosh, A. B., Black, J. et al. 2009, *Phys. Rev. C*, 80, 064611

Iglio, J., Shetty, D. V., Yennello, S. J. et al. 2006, *Phys. Rev. C*, 74, 024605

Ishizuka, C., Ohnishi, A., & Sumiyoshi, K. 2003, *Nucl. Phys. A*, 723, 517

Lamb, D. Q., Lattimer, J. M., Pethick, C. J., & Ravenhall, D. G. 1978, *Phys. Rev. Lett.*, 41, 1623

Lamb, D. Q., Lattimer, J. M., & Pethick, C. J. 1981, *Nucl. Phys. A*, 360, 459

Lattimer, J. M., Pethick, C. J., Ravenhall, D. G., & Lamb, D. Q. 1985, *Nucl. Phys. A*, 432, 646

Lattimer, J. M. & Swesty, D. F. 1991, *Nucl. Phys. A*, 535, 331

Ogul, R., Botvina, A. S., Atav U. et al. 2011, *Phys. Rev. C*, 83, 024608

Pienkowski, L., Kwiatkowski, K., Lefort, T. et al. 2002, *Phys. Rev. C*, 65, 064606

Prakash, M., Bombaci, I., Prakash, M. et al. 1997, *Phys. Rep.*, 280, 1

Rodionov, V., Avdeyev, S. P., Karnaukhov, V. A. et al. 2002, *Nucl. Phys. A*, 700, 457

Scharenberg, R. P., Srivastava, B. K., Albergo, S. et al. 2001, *Phys. Rev. C*, 64, 054602

Shen, H., Toki, H., Oyamatsu, K., & Sumiyoshi, K. 1998, *Nucl. Phys. A*, 637, 435

Souliotis, G. A., Botvina, A. S., Shetty, D. V. et al. 2007, *Phys. Rev. C*, 75, 011601

Sugahara, Y. & Toki, H. 1994, *Nucl. Phys. A*, 637, 557

Sumiyoshi, K., Yamada, S. Suzuki, H. et al. 2005, *ApJ*, 629, 922

Sumiyoshi, K. & Röpke, G. 2008, *Phys. Rev. C*, 77, 055804

Typel, S., Röpke, G., Klähn, T., Blaschke, D., & Wolter, H. H. 2010, *Phys. Rev. C*, 81, 015803

Viola, V., Lefort, T., Beaulieu, L. et al. 2001, *Nucl. Phys. A*, 681, 267

Wang, G., Kwiatkowski, K., Bracken, D. S. et al. 1999, *Phys. Rev. C*, 60, 014603